Ann. Geophysicae 17, 659–673 (1999) © EGS – Springer-Verlag 1999

Annales Geophysicae

First results from the hot plasma instrument PROMICS-3 on Interball-2

I. Sandahl[1], S. Barabash[1], H. Borg[1], E. Y. Budnik[2], E. M. Dubinin[2], U. Eklund[1], H. Koskinen[3], K. Lundin[1], R. Lundin[1], A. Mälkki[3], R. Pellinen[3], N. F. Pissarenko[2], T. Pulkkinen[3], and A. V. Zakharov[2]

[1] Swedish Institute of Space Physics, PO Box 812, SE-981 28, Kiruna, Sweden
E-mail: ingrid@irf.se
[2] Space Research Institute, Profsoyuznaya 84/32, 117 810 Moscow GSP-7, Russia
[3] Finnish Meteorological Institute, PO Box 503, FIN-00101 Helsinki, Finland

Received: 18 August 1998 / Revised: 23 October 1998 / Accepted: 26 October 1998

Abstract. The PROMICS-3 instrument on Interball-2 is nominally identical to the PROMICS-3 instrument on Interball-1. It performs three-dimensional measurements of ions in the energy range 4 eV–70 keV with mass separation and of electrons in the energy range 300 eV–35 keV. Interball-2 was launched on August 29, 1996, into an orbit with the same inclination as that of Interball-1, 63°, but with apogee at 20 000 km. In this study the PROMICS-3 instrument on Interball-2 is briefly described and examples of the first results are presented. Firstly, we report observations of upward moving molecular ions with energies of up to 700 eV at the poleward edge of the auroral oval. Previous observations of outflowing molecular ions have been at lower altitudes and lower energies. Secondly, we show observations of dawnside magnetosheath plasma injections. Using conjugate data from both PROMICS-3 instruments we have found dispersion structures above the morningside auroral oval, which occurred simultaneously with isolated "pockets" of magnetosheath plasma at a distance of $X_{GSM} = -14$ to $-12\,R_E$, which had been injected into the inner part of the low-latitude boundary layer. These isolated plasma structures were sites of strong field-aligned currents and are proposed to be the magnetospheric counterparts of the dispersion structures.

Key words. Magnetospheric physics (auroral phenomena; magnetotail boundary layers; instruments and techniques)

1 Introduction

Interball-1, also called the Interball Tail Probe, was launched on August 2, 1995. It was joined by Interball-2, or the Interball Auroral Probe about one year later, on August 29, 1996. The objective of the Interball project is to study the transport of solar wind plasma, energy and momentum through the magnetopause and the processes this transport gives rise to within the magnetosphere. A comprehensive description of the scientific problems targeted by Interball has been given by Galeev *et al.* (1995). By performing simultaneous measurements in the solar wind, in the magnetosheath, the magnetospheric boundary layers, and the tail at distances out to 31 R_E with Interball-1 and above the auroral ionosphere out to 20 000 km with Interball-2, new information concerning, for example, dynamical processes and the evolution of particle distributions can be obtained. Thanks to the orbital inclination of 63° for both spacecraft, information is also obtained at the high-latitude magnetopause with Interball-1, while for Interball-2 this inclination often allows scans more or less from west to east along the auroral oval.

Both Interball spacecraft are equipped with nominally identical PROMICS-3 instruments, which perform three-dimensional measurements of electrons and positive ions with mass separation. PROMICS is an acronym for Prognoz Magnetospheric Ion Composition Spectrometers, as PROMICS-1 and PROMICS-2 were flown on Soviet Prognoz satellites. The PROMICS-3 team consists of scientists from the Swedish Institute of Space Physics, IRF, in Kiruna the Space Research Institute, IKI, in Moscow and the Finnish Meteorological Institute, FMI, in Helsinki.

In the case of Interball-1, the three-dimensional capability is unique and PROMICS-3 is the first instrument to perform such measurements at the high-latitude magnetopause. The near-Earth region covered by Interball-2 has been much more thoroughly explored by several satellites. The more recent ones, such as Freja, FAST, and Polar have been able to perform excellent 3D measurements, in many cases with a time resolution superior to that of PROMICS-3. However, most of these measurements were made either at substantially lower or at much higher altitudes than Interball-2. In many

Correspondence to: I. Sandahl

co-operative studies the PROMICS-3 data obtained at 20 000 km is able to help bridge the gap between measurements in the ionosphere and measurements further out in the magnetosphere. In addition, PROMICS-3 on Interball-2 profits from the possibility of comparisons with its own sister instrument at higher altitudes.

In this work we first give a short description of the PROMICS-3 instrument. We then present examples of the initial results, firstly observations of upward moving molecular ions, and secondly, observations of dispersion structures which we interpret as results of injections of magnetosheath plasma through the tail magnetopause.

Upward moving molecular ions have previously been detected in the high-altitude auroral ionosphere by DE 1 up to 12 000 km altitude (Craven *et al.*, 1985) and by Akebono up to 10 500 km (Yau *et al.*, 1993). The ion species detected in the mass range around 30 amu were N_2^+, NO^+, and O_2^+. Typical energies in the dayside were 5–20 eV and in the nightside somewhat higher but still in the 10s of eV range. Observations of molecular ions are rare and are related to disturbed geomagnetic conditions. The molecular ion measurements presented were carried out at 600 eV, which is much higher than reported earlier. The Interball-2 observations were also obtained at a higher altitude than the previous measurements.

Dispersion structures above the morning-prenoon and postnoon-evening auroral oval outside the cusp have been studied using data from Viking by Woch and Lundin (1991, 1992) and by sounding rockets (Carlson and Torbert, 1980). The particle distribution of these structures and the locations where they are found are such that Woch and Lundin (1991, 1992) concluded that they are caused by transient penetration of magnetosheath plasma. However, no simultaneous measurements in the magnetosheath or low-latitude boundary layer, LLBL, were available at that time. There is a fairly wide agreement that the dispersion structures, also called plasma transfer events, PTEs, are indeed caused by magnetosheath plasma, but where and by what mechanism this plasma enters the magnetosphere remains controversial. The signature of the source distribution of the dispersion structures has not been unambiguously identified and it is also not understood how this source can be switched on and off to create clear-cut dispersion signatures. These questions are addressed here using simultaneous conjugate measurements above the auroral ionosphere by Interball-2 and in the dawnside LLBL by Interball-1.

2 The PROMICS-3 instrument on Interball-2

2.1 Basic design

The instrument PROMICS-3-Auroral on Interball-2, is almost identical to PROMICS-3-Tail on Interball-1 which has been described by Sandahl *et al.* (1995, 1997). The reader is referred to those papers for a more thorough description. Here we will only summarise the most important properties of the instrument, in particular those of importance for the data interpretation. A description of PROMICS-3-Auroral, originally in Russian, has also been given by Budnick *et al.* (1998).

The only nominal difference between PROMICS-3-Auroral and PROMICS-3-Tail is that the former is equipped with radiation-hardened circuits. Interball-2 spends much time in the radiation belts and is exposed to a much higher radiation dose than Interball-1. There are also differences in sensitivity, exact opening angles and exact energy levels, which have been found by calibration.

The hot plasma instrument PROMICS-3 consists of two units, the electron spectrometer MEPS (magnetospheric electron spectrometer) and the 3D ion composition spectrometer TRICS. MEPS-Auroral covers the energy range 300 eV–35 keV. The basic design is shown in Fig. 1. Electrons enter a large toroidal electrostatic analyser, ESA, and are measured by 8 channel electron multipliers, CEMs, placed in a half circle behind the electrostatic analyser. Mullard X955-BL CEMs were used.

The basic equation for the centre energy of the instrument is

$$\frac{W_i}{q} = \frac{R_m \Delta V_i}{2d} \tag{1}$$

where W_i is the centre energy for energy level i, R_m the mean radius of the analyser plates, d the plate distance, q the particle charge and ΔV_i the voltage difference $V_- - V_+$ between the analyser plates for energy level i.

The entrance plane of the electrostatic analyser is shown in Fig. 2. Also shown is the satellite spin axis, which is in the same plane, Only electrons entering from a limited range of angles with respect to the spin axis are able to reach each CEM. Figure 3 shows the result of a calibration of the relative transmission function for the MEPS-Auroral detectors as a function of viewing angle with respect to the spin axis. There is some overlap between the directions measured by each detector. The full unit sphere is covered in one spin. As the spin axis points towards the Sun, detector D12 measures essen-

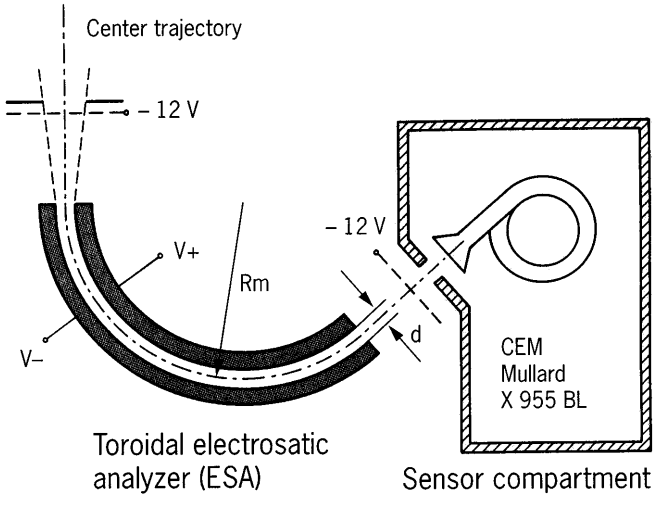

Fig. 1. General design principle of the electron spectrometer MEPS

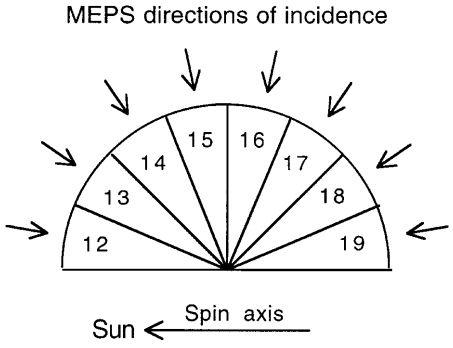

Fig. 2. Viewing directions for the different detectors of MEPS

tially anti-Sunward streaming electrons all the time, while D19 measures Sunward streaming electrons. A grid at −12 V at the instrument entrance rejects low energy electrons. The centre potential of the electrostatic analyser is kept at 0 V.

The design of the ion spectrometer TRICS is similar to that of MEPS, but, in addition, Wien filters or crossed field analysers, CFAs, are placed between the electrostatic analysers and the CEMs, as shown in Fig. 4. The combination of an electrostatic analyser and a velocity filter gives a mass per charge spectrometer. In the velocity filters the magnetic field is created by a pair of samarium-cobalt permanent magnets and the variable electric fields by a pair of flat electrostatic plates.

The centre energy is given by the same equation as for MEPS. The centre mass for mass level j and energy level i is obtained from Wien filter equation $v = E/B = \Delta V_{cj}/d_c B$ in combination with the energy per charge W_i/q from Eq. (1). It can be expressed as

$$\frac{m_{ij}}{q} = \frac{2W_i}{q}\left(\frac{d_c B}{\Delta V_{Cj}}\right)^2 \qquad (2)$$

v is the particle velocity, E is the electric field, B the permanent magnetic field and d_c the plate distance of the Wien filter. ΔV_{Cj} is the voltage difference for mass level j.

TRICS is divided into three subunits to improve the dynamic range. TRICS-1 nominally measures the energy range 4 eV–1.5 keV and contains the five detectors D1–D5. TRICS-2 measures the range 1–30 keV and contains the detectors D6–D10. The entrance planes of TRICS-1 and TRICS-2 are shown in Fig. 5. Note that the solar direction in this figure is opposite to the direction in Fig. 2 and thus anti-Sunward streaming ions are measured by detectors D5 and D10. TRICS-3 covers the energy range 5–70 keV. It contains only one detector, D11, and accepts particles from a wide range of angles centred around the perpendicular direction with respect to the spin axis. Figure 6 shows the calibrated relative transmission of TRICS 1, 2, and 3. The velocity filters also act as collimators and as a result there is very little overlap between the fields of view of the detectors within each subunit.

TRICS-1, 2, and 3 are stacked to save mass and volume. TRICS-3 has a very large pair of analyser plates which gives a very good angular and energy resolution but less sensitivity. TRICS-2 is intermediate and TRICS-1 has small plates, the largest geometric factor, but not as good angular and energy resolution. Because of the large geometric factor TRICS-1 is also somewhat sensitive to UV-light, and sunpulses therefore appear in detectors D5, D4, and D3.

All five velocity filters of TRICS-1 share one power supply and another power supply feeds all TRICS-2 velocity filters. The ideal voltage settings for the velocity filters are different for different detectors of the same subunit and the settings used are a compromise. At the lowest energy levels a very precise velocity filter setting is required and due to a certain mismatch the sensitivity of the spectrometers is lower, at these levels, than planned. This should be understood when interpreting the data.

The velocity filter voltage settings are based on calibrations carried out at fixed voltage levels. These settings give the nominal mass levels. When PROMICS-3 is operated in space the mass peaks for some detectors and mass levels are shifted slightly from the nominal ones due to time constants of the instrument and the imperfect matching of the energy filters and velocity filters described in the previous paragraph.

A summary of PROMICS-3 instrument properties is given in Table 1.

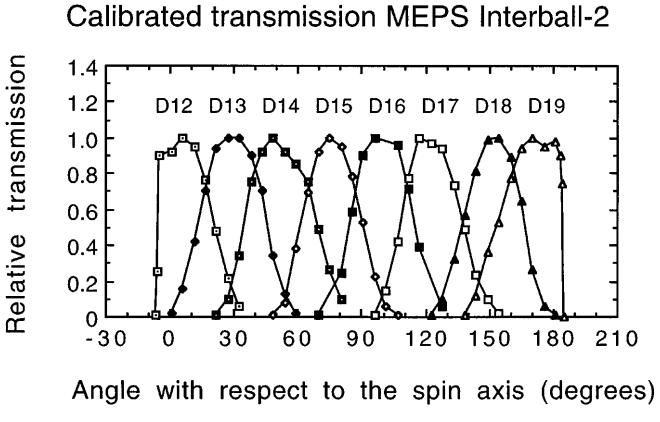

Fig. 3. Calibrated relative transmission of the MEPS detectors as a function of incidence angle with respect to the satellite spin axis

2.2 Measurement modes

PROMICS-3 has four different measurements modes, but the ones used most are mode A and mode F. These modes are described in Fig. 7. MEPS has only one measurement mode.

For each TRICS mode the top panels show the selected energy per unit charge and the bottom panel the selected mass per unit charge as a function of time. In mode A there are four 32 level energy sweeps for four different preselected masses followed by two 32 level mass sweeps for preselected energies. The preselected mass and energy levels can be changed by telecommands. Default masses are 1, 2, 4, and 16 amu per unit charge.

The sampling time at each energy and mass level is 50 ms. One complete measurement cycle in mode A

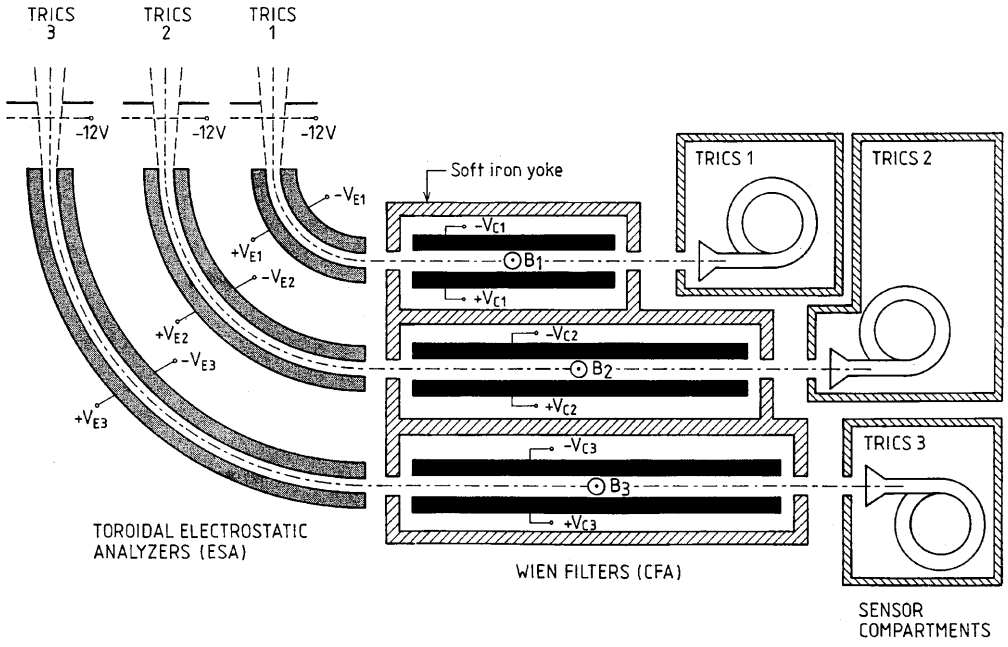

Fig. 4. General design principle of the positive ion mass spectrometer TRICS

takes 9.6 s. Thus a 120 s spin covers 12 cycles. Between each cycle there is a lag time called "sweep delay" chosen so that the 12 measurement cycles are evenly distributed around the spin. The sweep delay is calculated by the onboard computer using the spacecraft spin pulse as input, and is updated every spin.

Some TRICS data have been collected in the C mode. The C mode has the same cycle duration as the A mode, but has energy sweeps for 6 preselected masses and no mass sweeps.

Mode F is designed for fast measurements. The measurement cycle takes 3.2 s and contains energy sweeps of 16 levels for four preselected masses. It is used to study for example boundary crossings. The F mode is only used together with the telemetry mode D, which is described in Sect. 2.3.

The MEPS mode has a cycle of 3.2 s regardless of the TRICS mode. It contains 64-energy levels, but these are immediately integrated to give 32 energy levels or less depending on the telemetry mode. It is necessary to perform the measurements at a higher number of levels due to the small energy bandwidth of the instrument.

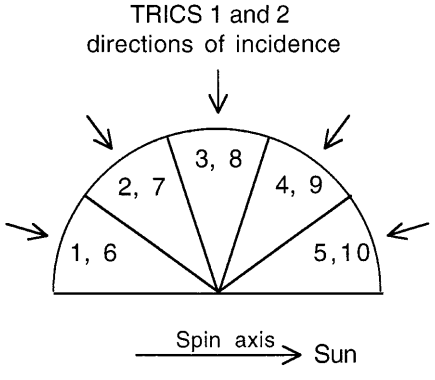

Fig. 5. Viewing directions for the different detectors of TRICS and the direction of the satellite spin axis

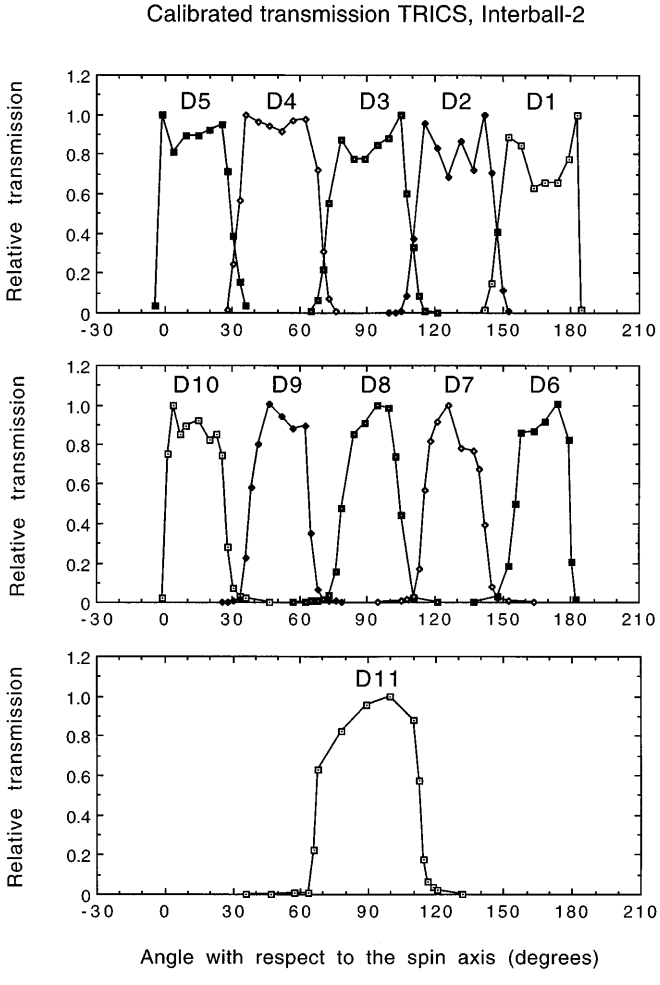

Fig. 6. Calibrated relative transmission of the TRICS detectors as a function of incidence angle with respect to the satellite spin axis

Table 1. Summary of PROMICS-3 instrument properties

	MEPS	TRICS		
Particle species:	Electrons	Ions 1–56 amu, mass separation		
Weight (kg):	3.2	12.6		
Power consumption (W):	2	11		
	MEPS	TRICS-1	TRICS-2	TRICS-3
Energy range (keV):	0.3–35	0.004–1.5	1–30	5–70
Number of sensors:	8	5	5	1
Total field of view (degrees):	3×180	8×180	4×180	1×47
Field of view per sensor:	3×35	8×36	4×27	1×47
Geometric factor at 1 keV (cm^2 sr):	6×10^{-5}	1×10^{-3}	8×10^{-5}	3×10^{-5}
$\Delta E/E$ (FWHM):	0.07	0.19	0.10	0.06
$M/\Delta M$ (FW) for H+:		3 (1 keV)	9 (6 keV)	16 (12 keV)
Calculated moments:	Density, mean velocity vector, pressure tensor, energy flux			
Temporal resolution:	120 s (= one spin) for full distribution (240 s in slow mode)			
Data production rate	16 bps (slow), 40 bps (medium), 384 bps (fast), 1900 bps (direct)			

2.3 Telemetry modes and data compression

PROMICS-3 has rather severe telemetry and onboard data storage constraints and, for this reason data compression is necessary. The data compression is carried out by onboard data processing, such as integration, averaging and calculation of plasma moments. A number of different schemes for doing this have been adopted, and these schemes are termed telemetry modes. For each TRICS mode there are four telemetry modes, D (direct) which gives an output of 1900 bps, F (fast) with 384 bps, M (medium) with 40 bps and S (slow) with only 16 bps. The complete mode names consist of three letters, for example AED, where the first letter is the measurement mode and the last the telemetry mode.

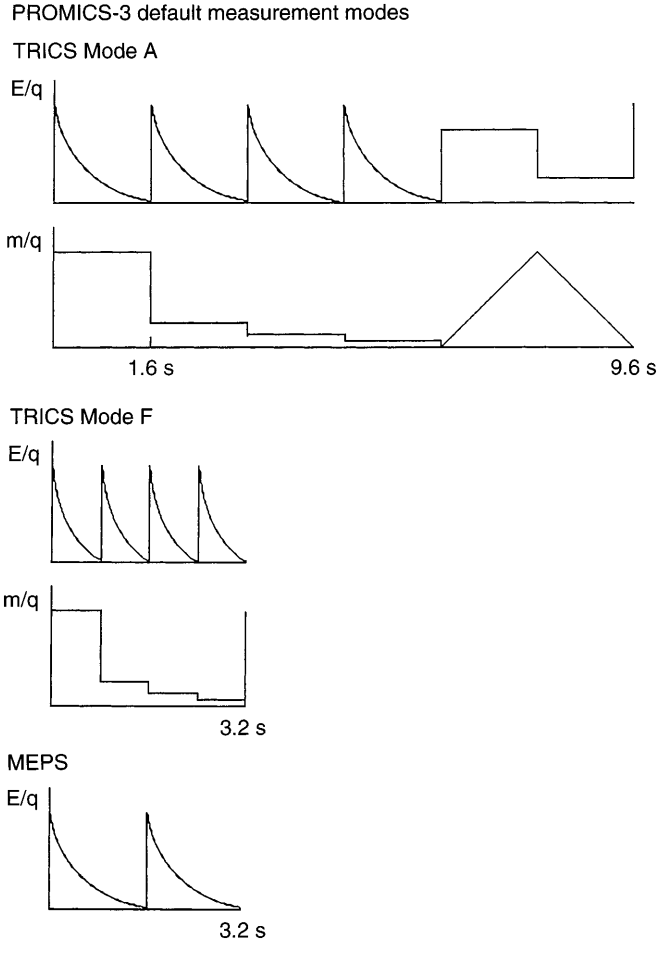

Fig. 7. Energy and mass sweeps of the most frequently used measurement modes

In order to make optimum use of the data storage quota each data-taking session is carefully planned in advance taking into account for example expected boundary locations, locations of magnetospheric regions and predetermined satellite conjunctions. In the data plots there are quite often mode changes, and in many cases the data shown represent averages over energy, angular bins, spins and even pairs of detectors. To interpret the data it is necessary to have some understanding of how the averaging is done in different modes, and therefore a brief description is given.

2.3.1 D telemetry modes. The output from PROMICS-3 is a combination of energy spectra, mass spectra and plasma moments. In the D telemetry modes there are energy and mass spectra from all individual detectors. In the AED mode the only compression is averaging over two 9.6 s cycles for two of the masses, detector 11, and the mass spectra. In FED mode data from detectors D2, D4, D7, D9, and D11 are averaged over two cycles, while for the remaining detectors all data are telemetered. Since almost all information is telemetered no moments are calculated onboard the satellite.

2.3.2 F telemetry modes. In the F telemetry modes some energy spectra are averaged to 16 energy levels for each subunit. Data from TRICS detectors are also time-averaged so that most detectors give four values per spin and detectors D2, D4, D7, and D9 give two values per spin. There are spin-averaged mass spectra from most detectors and no mass spectra at all from detectors D2, D4, D7, and D9.

The electron data are averaged in time according to the same principles as the ion data. In addition, data from detectors D13–D18 are averaged in pairs.

Information from all individual detectors appear as onboard-calculated moments. Thirteen moments are calculated; density, velocity vector (three components), pressure tensor (six components) and energy flux vector (three components). The principles of the moment calculation were presented in Sandahl *et al.* (1995). The temporal resolution of the moments in the F modes is one value per spin.

2.3.3 M and S telemetry modes. In the M and S telemetry modes a much larger fraction of the data stream is devoted to moments. In M modes the temporal resolution of the moments is one value per spin and in S modes one value per two spins. All 13 moments are obtained for two masses and for the remaining masses there is a reduced set of moments; the density the velocity vector and the magnitude of the squared velocity.

The energy spectra have only eight levels per subunit, but since there are three subunits we still receive ion spectra of 24 levels from the complete instrument. The data storage constraints only allow spectra from some of the detectors and we have chosen the ones looking most closely to the spin axis, that is ion detectors D1, D6, D5, D10 and electron detectors D12 and D19, and the ones looking transverse to the spin axis, that is ion detectors D3, D8, and D11 and electron detectors D15 and D16. The data from the detectors looking almost parallel or anti parallel to the spin axis are spin averaged giving one value per one or two spins in M modes depending on the mass and one value per four spins in S modes. For transverse detectors the temporal resolution is the same, but the ion data are averaged into four angular bins. It is thus not strictly correct to present data from these detectors as a time series although that is what we actually do.

Mass spectra in M and S modes are obtained from the same detectors as the energy spectra. In S modes the temporal resolution is four spins, in M modes two spins. Data from the detectors quasi parallel to the spin axis are spin averaged, data from the transverse detectors are binned into four angular bins.

3 First results

Two examples of results from PROMICS-3-Auroral are given. In addition, observations of the cusp have been presented by Budnick *et al.* (1998) and of evening-side dispersion structures during the 10–11 January 1997 magnetic storm by Sandahl *et al.* (1998).

3.1 Energetic molecular ions at the poleward edge of the auroral oval

3.1.1 Data description. Figure 8 shows the position of Interball-2 on January 27, 1997 between 19 and 22 UT.

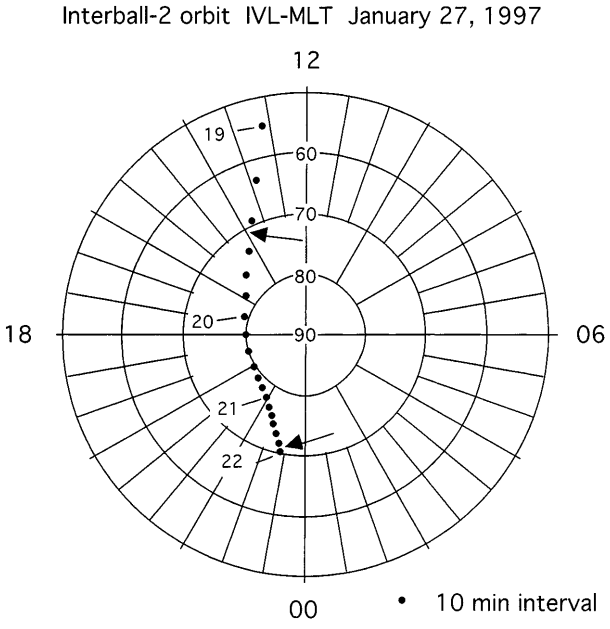

Fig. 8. Orbit of Interball-2 on January 27, 1997

The satellite came from the dayside to the nightside, crossing the auroral oval at about 14 and 23 MLT. The arrows in Fig. 8 mark the equatorward edges of the polar cap as determined from the PROMICS-3 ion and electron data.

Figure 9 shows PROMICS-3 data taken between 2130 and 2204 UT, that is in the nightside part of the polar cap and poleward part of the nightside oval. PROMICS-3 was measuring in the AEF mode, which has a time resolution of one spectrum per 30 s or four spectra per spin.

The two top panels show electrons in the energy range 0.3–35 keV and protons in the energy range 1–30 keV measured transverse to the satellite spin axis. The polar cap was fairly void of particles everywhere, also in the part not shown in Fig. 9. The geomagnetic disturbance level was somewhat elevated, with $K_p = 4$ between 21 and 24 UT, so this is exactly as expected. The poleward boundary of the auroral oval was crossed at 2150 UT and when PROMICS-3 was switched off at 2204 UT Interball-2 was still in the auroral oval.

Panels 3–6 of Fig. 9 show energy spectra for H^+, He^{++}, He^+, and O^+ in the transverse direction for energies up to 1.5 keV. This detector samples upward moving ions once per spin. At 2153 UT upward moving low-energy O^+ (panel 6) and He^{++} (panel 4) ions were detected. One spin later there was intense upward moving H^+, He^+, and O^+ at up to 1.5 keV.

Panels 7 and 8 contain mass spectra for 100 and 600 eV obtained from the same detector as panels 3–6. Each mass spectrum represents one spin. At 2153 UT all upward moving ions had energies below 100 eV and were not recorded in the mass spectra. During the next spin, however, protons were measured at both 100 and 600 eV in agreement with the wide energy spectrum. At 600 eV there were also a number of additional peaks,

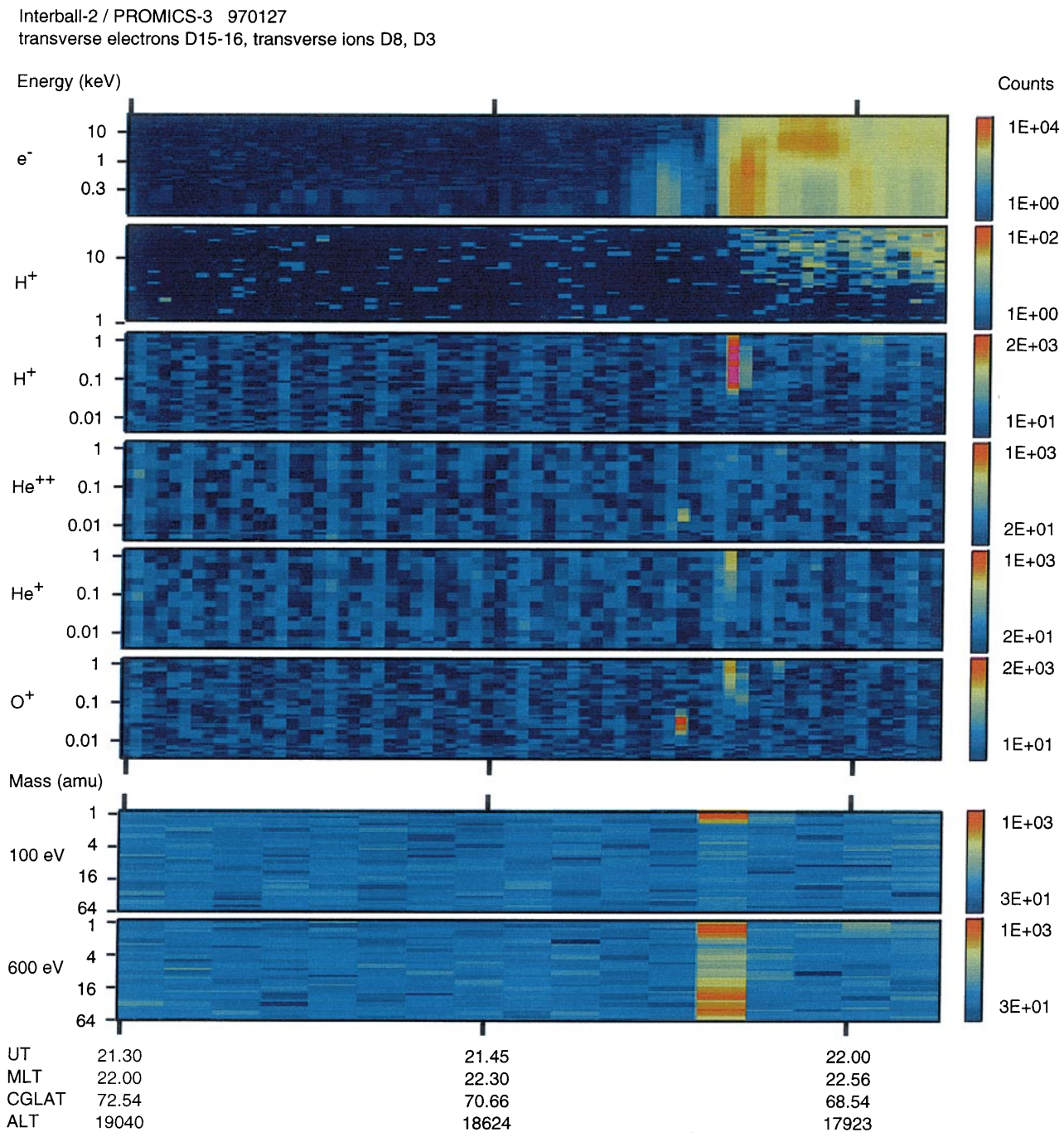

Fig. 9. Spectrogram from January 27, 1997. The *six upper panels* are energy spectrograms of electrons and different ion species, the *two lower panels* mass spectrograms at two different energy levels. Upward moving molecular ions were detected at 2150 UT

one which we identify as O^+ and one of approximately the same intensity at about 32 amu.

A line plot of the mass spectrum at 600 eV is shown in Fig. 10. The H^+, O^+, and heavier ion peaks are all quite distinct.

Since the mass spectrum was obtained at a fixed energy level, which was kept constant for a long time, 1.6 s, the energy determination is very reliable. The energy bandwidth of this detector is 19% FWHM, so this means that the mass peaks represent energies between somewhat more than 500 and 700 eV.

The O^+ peak appeared at mass level 24, which nominally corresponds to 21 amu. Partly this is because the actual masses measured by this detector are somewhat lower than the nominal ones. Reasons for this were described in Sect 2.1. But in this particular case we should also expect a mass level shift, since, according to the energy spectrum, the O^+ ions have energies in the upper part of the energy window. This is obvious from Eq. (2). From the asymmetry of the peak we may conclude that there was also a contribution from some lighter ions, most likely N^+.

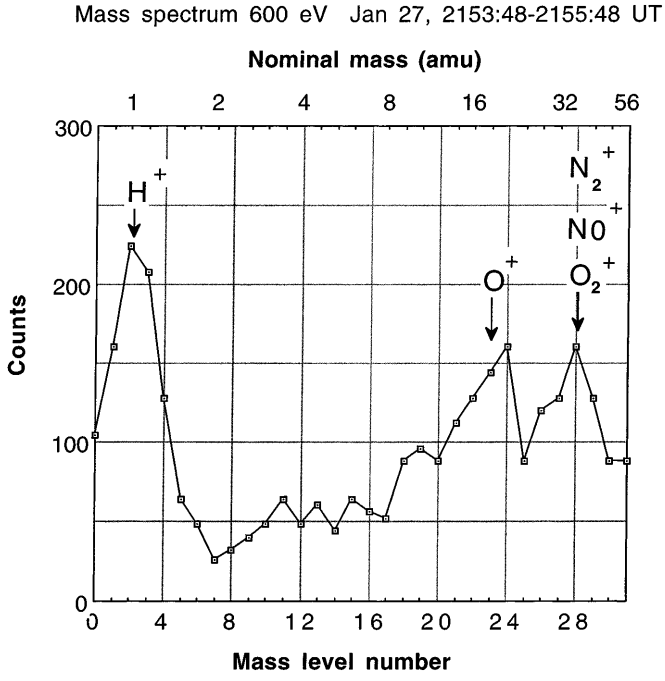

Fig. 10. Mass spectrum obtained at 2153:48–2155:48 UT on January 27, 1997

The third peak in the 600 eV mass spectrum maximizes at mass level 28. This peak probably consists of a combination of molecular ions such as N_2^+, NO^+, and O_2^+.

From our data it is actually not possible to determine with certainty that these molecular ions are upward moving. The mass spectrum is a spin average, and no energy spectrum was obtained at this mass level. However, it seems most likely that molecular ions were accelerated upward together with the atomic ions.

3.1.2 Discussion. The observations presented here are in good general agreement with results on molecular ions obtained earlier. The main difference is that the energy is much higher than found previously in the high altitude auroral ionosphere.

Molecular ions have been found in the altitude range 500–2500 km by OGO6 (Taylor, 1974), ISIS 2 (Hoffman *et al.*, 1974) and ACTIVNY (Förster *et al.*, 1992). In the high altitude ionosphere they have been measured in the dayside polar cap by DE 1 up to 12 000 km (Craven *et al.*, 1985) and in both the dayside cusp and nightside auroral oval by Akebono (Yau *et al.*, 1993). The mode used in the Akebono study measured at a maximum energy of 70 eV. Yau *et al.* (1993) reported that typical dayside energies were 5–20 eV and that typical nightside energies were larger but no energy range was specified. It is however, quite clear that very efficient energisation of the molecular ions must take place. In the equatorial plane in the outer ring current at $L = 7$ AMPTE IRM detected molecular ions with energies of 80–230 keV during a magnetic storm (Klecker *et al.*, 1986). In all these studies it was agreed that the source of the molecular ions is the ionosphere.

The altitude of the PROMICS-3 measurements was 18 000 km and the energy of the molecular ions measured there was 500–700 eV. Thus these ions had gained more energy than the ions measured by Akebono.

All previous observations of molecular ions in the high altitude ionosphere and the magnetosphere have been made during magnetically disturbed conditions. During our event K_p was 4 and the activity had been elevated since the previous day with a maximum K_p of 5−. In the Akebono study 440 passes were surveyed and molecular ions were found in 3% of them, typically during prolonged periods of enhanced geomagnetic activity. In Interball-2 data molecular ions measurements are also rare, but the example presented here is not unique. We have found molecular ion events both in the dayside and in the nightside.

The suprathermal mass spectrometer on Akebono could determine the masses very accurately. Molecular ions were at times responsible for as much as 15% of the total ion content. The dominating molecular species were N_2^+ and NO^+, which appeared in roughly equal numbers, while there was one order of magnitude less O_2^+. At the same time there would always be more N^+ ions than normal with the ratio N^+ and O^+ in the range 0.5–1. In our case it is very likely that the second peak in Fig. 10 is dominated by O^+ with some contribution from N^+, while the third, molecular peak is dominated by N_2^+ and NO^+ with some contribution from O_2^+ . This can explain some of the difference in the shapes of the peaks and the different shifts with respect to the nominal mass scales. The molecular contribution in Fig. 10 to the total ion flow is even stronger than in the cases found by Akebono, making up almost 30% of the measured flux. It must, however, be taken into account that temporal variations may have occurred while the spectrum was measured, and that the sensitivity of TRICS is energy dependent. In the case of O^+ we are just measuring the low energy tail of the distribution, as explained above.

Akebono found the nightside molecular ions inside and equatorward of the auroral oval. Our observation was confined to the poleward part of the auroral oval and was accompanied by electron precipitation.

3.2 Conjugate measurements by Interball-1 and Interball-2 of injection structures in the morningside

3.2.1 Data description. One of the main ideas behind the Interball project is to perform conjugate measurements above the auroral oval and the magnetospheric boundary layers. One opportunity for such measurements came on October 4, 1996. This was a magnetically quiet day with *Kp* at 1 or 2 most of the time. The WIND spacecraft was in the solar wind until just before 01 UT and measured a northward IMF of a few nT and a solar wind velocity of about 500 km/s. WIND then crossed the magnetosheath until about 0420 UT and during that time measured southward B_Z during 0300–0320 and 0400–0410 UT, which may be taken as signs of weak southward turnings of the interplanetary

magnetic field. IMP-8 was all this time in the geomagnetic tail.

Figure 11 shows a 24 h plot of data from Interball-1. At the beginning of the session PROMICS-3-Tail was in the AEM mode, but between 01 and 06 UT it was in the high time resolution mode AEF. The remaining time was spent in the minimum resolution AES mode. Unfortunately PROMICS-3 did not give any data in the 1–4 keV energy range, but information on this is available from the CORALL instrument (A. Fedorov, personal communication, 1998).

Interball-1 had entered the magnetospheric tail on the dawnside close to the equatorial plane at X_{GSM} about -16 R_E. It crossed the LLBL obliquely, travelling towards the Earth. The first magnetopause crossing took place on October 3 before 22 UT, but there was also a brief excursion to the magnetosheath between 0100 and 0115 UT on October 4.

Interball-1 then travelled through the LLBL, characterised by anisotropic particle distribution functions and a lack of ions above 5 keV as seen in detector D11, and gradually entered the plasma sheet with its higher fluxes of ions measured by D11. Interball-2 performed measurements above the dawnside auroral oval during two time intervals which are marked 1 and 2 in Fig. 11.

The footpoints of October 4 of Interball-1 and Interball-2 calculated for $Kp = 3$ are shown in Fig. 12. This calculation was carried out using a combination of the Tsyganenko 89 model and IGRF. A colour coding has been used to indicate regions and features identified in the particle data and these will be discussed later. Since the actual disturbance level on this day was less than was used in Fig. 12, the field lines crossed by Interball-1 may be expected to map even further poleward than shown in the figure. During pass 1 of Interball-2 *Kp* went from 1 to 2- and during pass 2 from 2+ to 3−.

The footpoints of Interball-1 make a J-shape reaching down to about 74° corrected geomagnetic latitude. During the latter part of the interval Interball-1 was in the Southern Hemisphere. Two arrows along the trace mark the times of the two Interball-2 passes. According to Fig. 12 the first Interball-2 pass, marked 1, had its foot point equatorward of Interball-1 and the second one, marked 2, was poleward. It is well known that foot point calculations such as this one must be used with great caution. On the other hand, mapping may still be useful during times of low substorm activity, as was the case here, in particular during pass 1 of Interball-2.

Figure 13 shows the proton measurements during the time period 01–06 UT by Interball-1 in greater detail. The large amount of structure is striking. Until just before 3 UT the dominant feature is the magnetosheath-like appearance of the protons. The most intense flux was measured by D5 showing a mainly anti-Sunward flow direction. After 3 UT protons instead appeared in the transverse and Sunward directions most of the time, while there was an almost total lack of ions in the anti-Sunward direction.

In the region dominated by the magnetosheath-like population, pockets of the transverse-Sunward flowing population were observed in a few places. These have been marked by arrows underneath the spectrogram. When this population appeared, there was a simultaneous dropout of the magnetosheath-like population. After 3 UT the situation was reversed. Isolated pockets of magnetosheath-like particles, marked by arrows above the spectrogram, appeared with simultaneous dropouts of transverse-Sunward protons. Regions with large amounts of magnetosheath-like plasma were probably encountered until after 7 UT, judging from

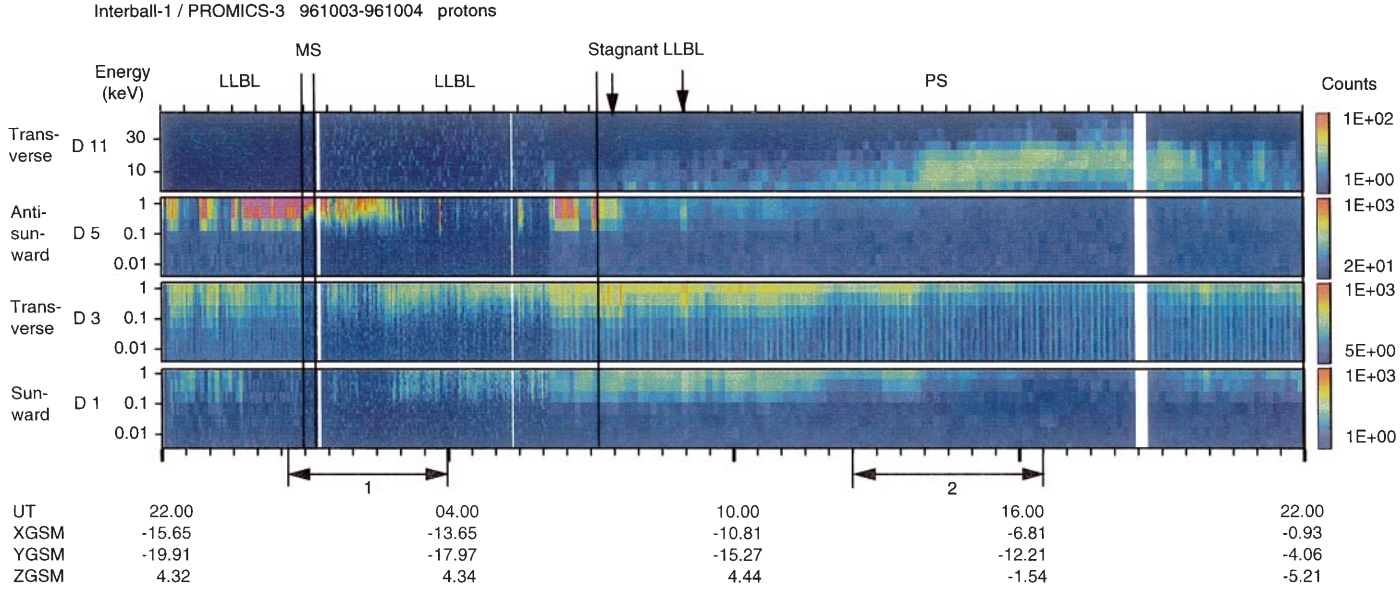

Fig. 11. Spectrogram from Interball-1 covering 24 h from 22 UT on October 3 to 22 UT on October 4, 1996. During this time nearly conjugate measurements were performed with Interball-1 and Interball-2. Interball-1 was inbound and spent the first part of the period in the dawnside flank magnetopause and LLBL region. The *periods* of PROMICS-3 measurements on Interball-2 are *marked below* the spectrogram

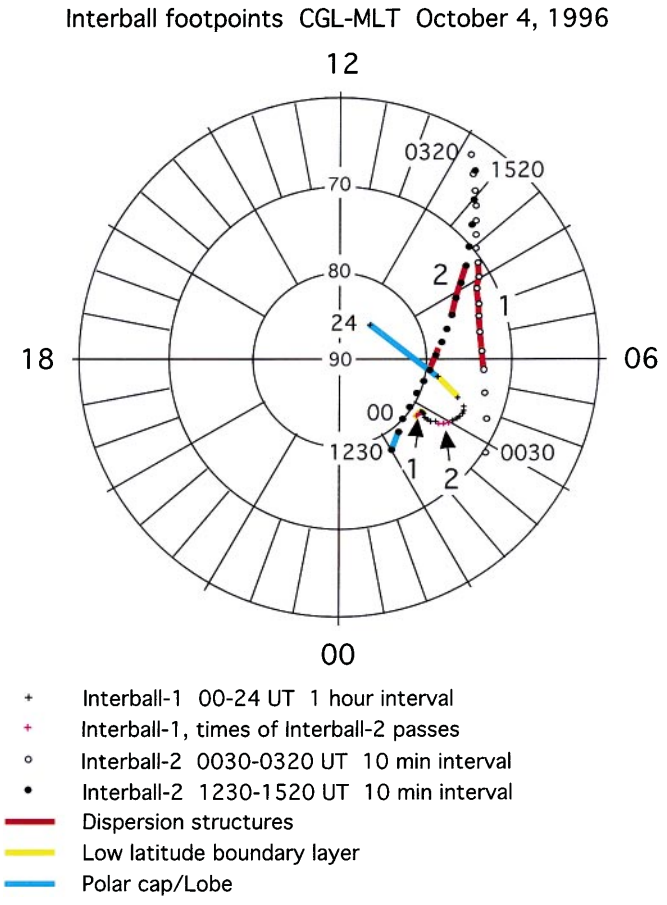

Fig. 12. Footpoints of the orbits of the two Interball satellites on October 4, 1996

the high fluxes measured by detector 5, which are shown in Fig. 11.

Just before 03 UT there was also a change in the character of the magnetic field, which became less rapidly fluctuating.

The width of the mainly magnetosheath-like region in the Y_{GSM}-direction was of the order 1.5 R_E while the region with mainly transverse-tailward flow was about 2 R_E.

At 0710 Interball-1 entered the plasma sheet, but also in this region there were isolated pockets of different plasma characteristics. These were encountered at about 0730 and 0900 UT. Here the average energy was lower than in the surroundings and there was a marked anisotropy in the fluxes measured in the transverse direction. We interpret these as pockets of stagnant LLBL-plasma.

Protons and electrons measured by PROMICS-3-Auroral during the first pass on October 4 are shown in Fig. 14. Interball-2 passed approximately along the morningside oval from 04–10 MLT. PROMICS-3 was in the AEF mode. Between 0053 and 0204 UT several dispersion structures were observed, approximately in the energy range 0.1–1.5 keV. They were found in the corrected geomagnetic latitude range 71–74° and at about 06–08 MLT. They are most clearly seen in the transverse directions measured by detector 3, but also in the Sunward streaming protons. They appeared more or less simultaneously with the plasma sheet protons with energies of 5–20 keV measured by detectors 8 and 11.

The dispersion structures were overlapping. The time difference between the arrival of the 1.5 and the 0.1 keV protons was about 12–17 minutes; in a stationary case this corresponds to a distance of 15–21 R_E. The longer time difference appeared for the most tailward dispersion structures.

Dispersion structures were also measured during the more poleward second Interball-2 pass between 79 and 72° corrected geomagnetic latitude. Data from detectors 8, 3, and 15–16 are shown in Fig. 15, panels 1, 2, and 3. Upward moving protons were detected in the same region as the dispersion structures, as well as poleward of it, and there were also weak fluxes of plasma sheet protons. For these dispersion structures the source region appeared to be even closer than 15 R_E.

3.2.2 Discussion. Careful studies of the properties of dispersion structures above the dayside auroral oval away from the cusp were carried out by Woch and Lundin (1991, 1992) using data from the Viking satellite obtained at altitudes up to 13 500 km. There is no doubt that the dispersion structures seen by PROMICS-3-Auroral are of the same type although the temporal resolution of the PROMICS-3 data is not as good as that of Viking. PROMICS-3, on the other hand, has better 3D coverage, and better separation of the different ion species.

Woch and Lundin (1991, 1992) showed that the plasma responsible for these dispersion structures most likely originates from the magnetosheath. They concluded that the structures are the ionospheric signatures of transient boundary layer processes and therefore called them injection events. The magnetosheath origin was suggested by the reconstructed source spectra.

Injection events were found to be very common. They appeared in a wide region both in invariant latitude and magnetic local time, with the highest probability between the trapping boundary and the poleward boundary of plasma sheet particles. In this latitude range they were found in more than 50% of the passes, and this means that the mechanism responsible for these events must be very important. The probability of occurrence had two maxima, one at 8 and one at 16 MLT.

Frequently boundary layer electrons were observed at the same time as the injection events. Most of the events were found in the region where plasma sheet particles are also present and it was concluded that they were usually, but not always, on closed field lines.

►

Fig. 13. Spectrogram and magnetic field data from Interball-1 showing the period between 0100 and 0600 UT on October 4, 1996. Two types of plasma alternate. Until about 0300 UT the plasma was mainly of a magnetosheath-like type and was streaming tailward. After that time the plasma was more plasmasheet-like and moved mainly in a transverse and Earthward direction. Arrows above the spectrogram mark isolated pockets of tailward streaming plasma and below of transverse-Earthward streaming plasma

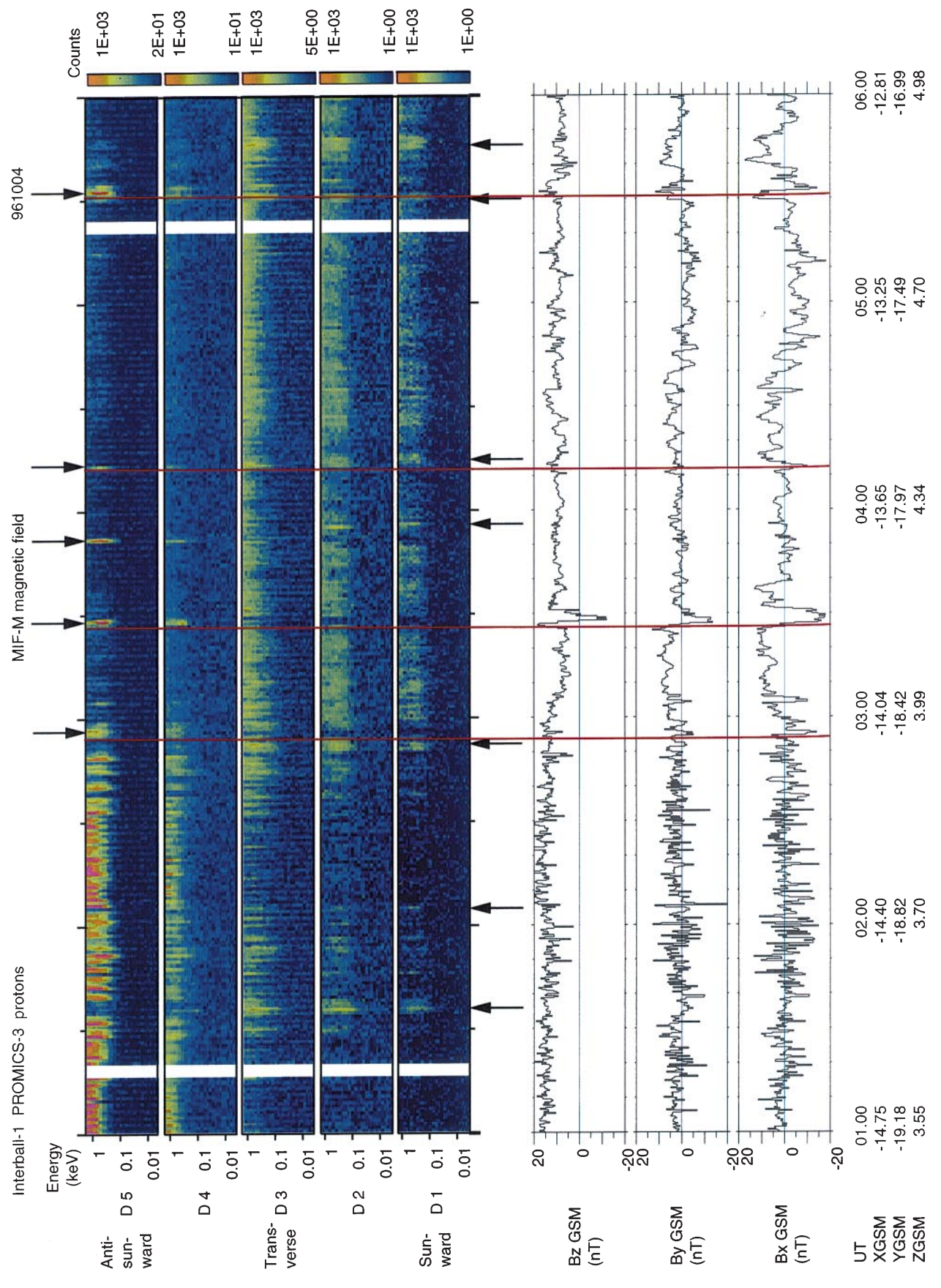
Interball-1 PROMICS-3 protons
MIF-M magnetic field
961004
Counts
1E+03
2E+01
1E+03
1E+01
1E+03
5E+00
1E+03
1E+00
1E+03
1E+00
Energy (keV)
Anti-sun-ward
Trans-verse
Sun-ward
D 5
D 4
D 3
D 2
D 1
1
0.1
0.01
Bz GSM (nT)
By GSM (nT)
Bx GSM (nT)
20
0
-20
UT
XGSM
YGSM
ZGSM
01.00
-14.75
-19.18
3.55
02.00
-14.40
-18.82
3.70
03.00
-14.04
-18.42
3.99
04.00
-13.65
-17.97
4.34
05.00
-13.25
-17.49
4.70
06.00
-12.81
-16.99
4.98

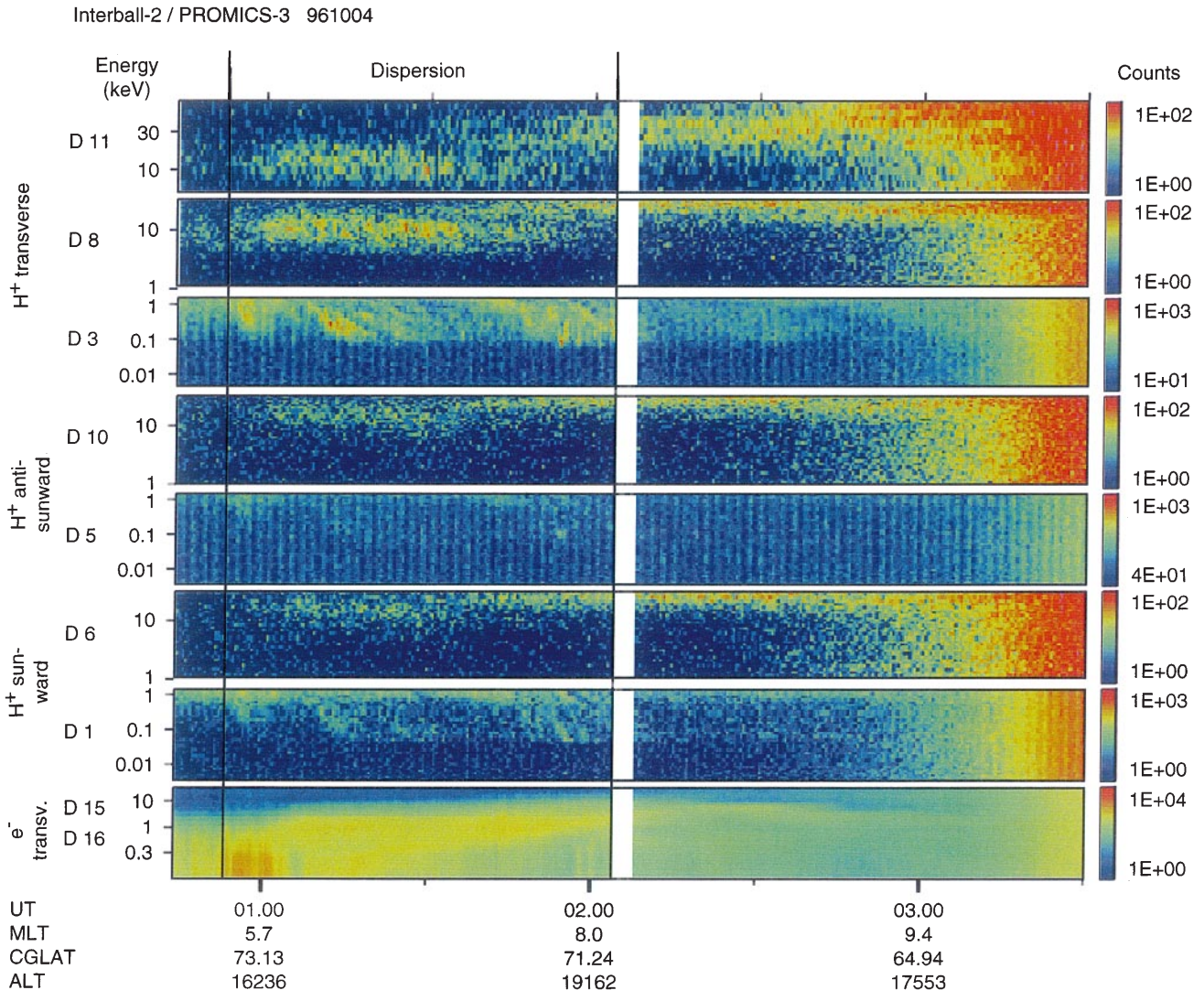

Fig. 14. Spectrogram from Interball-2 showing the period between 0040 and 0330 UT on October 4, 1996. Dispersion structures were detected between 0053 and 0204 UT

A very important property of the injection events is that, in order to create the observed signature, the source must first switch on and then off. This is somewhat reminiscent of the behaviour of pulsating aurora, which, however, occurs at much higher particle energies.

The PROMICS-3-Auroral observations of dispersion structures agree very well with the Viking observations of injection events. The events are observed at the same time as protons and electrons of the plasma sheet. Our earliest observations start a little before 06 MLT which is the earliest local time investigated in the Viking study. The high-latitude event at 1330 UT during pass 2 is short-lived and not as easy to see, just as was described for Viking.

The Interball-2 passes occurred at quite different latitudes and dispersion structures were seen in both passes (Figs. 14 and 15). From Viking we know that injection events are very common. The geomagnetic activity level did not change very much during the time between the passes. Therefore it is a reasonable assumption that dispersion structures were widespread in the dawn and prenoon sector. The clearest dispersion structures were seen in the more equatorward part of this region where plasma sheet plasma and even more energetic ring current plasma was present, and we thus conclude that they were on closed field lines.

We will now turn to the PROMICS-3-Tail data. We must at first admit that we cannot claim to have perfectly conjugate measurements. Interball-1 crossed the magnetopause a little bit too far tailward for ideal conjunction. During the high-resolution measurement interval 01–06 UT of Interball-1 the simultaneous Interball-2 pass went equatorward of the Interball-1 foot point and PROMICS-3-Auroral measured dispersion structures equatorward and dayward of it. About 12 h later PROMICS-3-Auroral began to measure dispersion structures at approximately the latitude where Interball-1 had found the magnetopause, but then the Interball-1 footpoint was equatorward as well as nightward of Interball-2. On the other hand, it is not

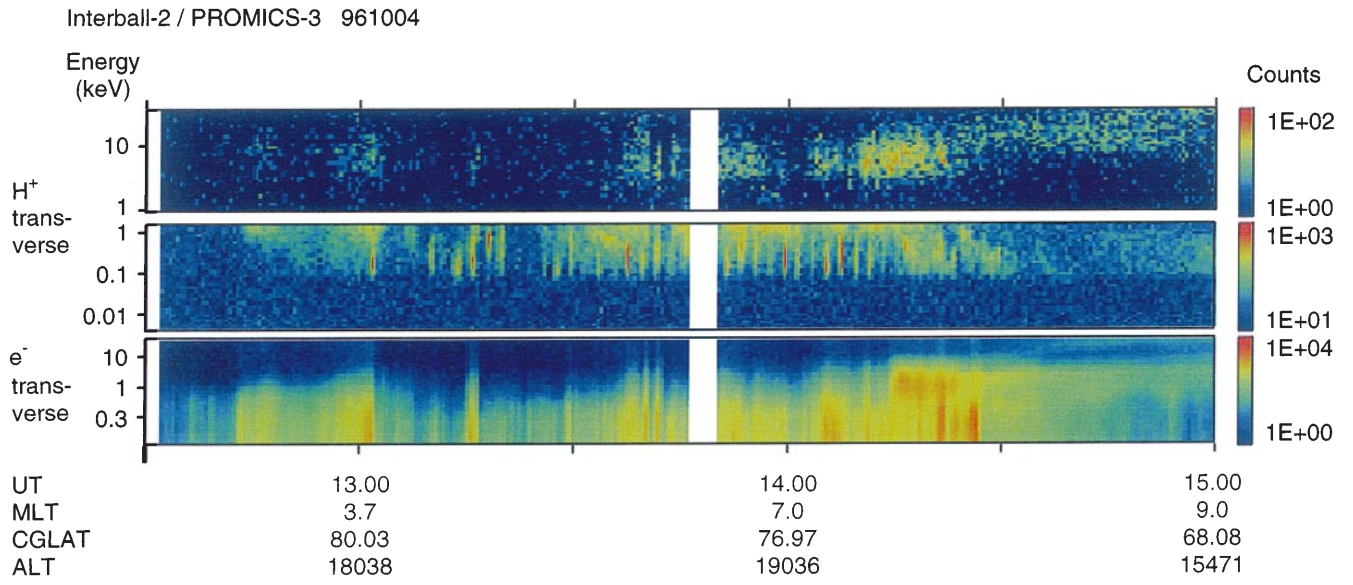

Fig. 15. Spectrogram from Interball-2 showing the period between 1230 and 1500 UT on October 4, 1996. Dispersion structures were detected between 1330 and 1440 UT

unreasonable to assume that the general character of the LLBL at $X_{GSM} = -15$ to $-13\,R_E$ was not very much different from $X_{GSM} = -5$ to $-10\,R_E$.

A very clear review of the properties of LLBL at the flanks of the magnetosphere is given by Scholer and Treumann (1997). It is a magnetospheric region at low latitudes just inside the magnetopause in which a large fraction of the plasma is tailward flowing and has properties similar to those in the magnetosheath. Some authors use the term LLBL for the entire region between the magnetopause and the plasma sheet (e.g. Fujimoto *et al.*, 1998) while others reserve it for the outermost region with tailward flow (Sckopke *et al.*, 1981; Paschmann *et al.*, 1990). In this study we use the wider definition.

The properties of the LLBL in the magnetotail have been investigated with ISEE 1 and 2 for $X_{GSM} > -15\,R_E$ (Mitchell *et al.*, 1987; Williams *et al.*, 1985; Traver *et al.*, 1991). More recently excellent measurement have been made with Geotail (Fujimoto *et al.*, 1997, 1998) and Interball-1 (Sauvaud *et al.*, 1997; Nemecek *et al.*, 1997; Savin *et al.*, 1997). The structure of the tail LLBL is quite complex and still not fully understood (Fujimoto *et al.*, 1997).

The large-scale picture given by Figs. 11 and 13 is that the region we have designated LLBL is a mosaic of two different types of plasmas, tailward flowing plasma dominating until 0300 UT and transverse-Earthward flowing plasma with more plasmasheet-like properties dominating between 3 and 7 UT. In the terminology used by Sckopke *et al.* (1981) the region before 03 is called LLBL while the region after is called the halo-region. Williams *et al.* (1985) in a study of particles above 24 keV used the term stagnation region for the halo region. Fujimoto *et al.* (1998) used the terms outer LLBL or sheath-like region and inner LLBL or mixing region to emphasise their properties.

More important than the names used for the two regions are the properties of the boundary between them. Several authors have interpreted the alternating plasma types as a signature of a wavy boundary caused by a Kelvin Helmholz instability. Such an interpretation is problematic in the event presented here. In the sheath-like outer LLBL the pockets of mixing region plasma are very narrow, and so are the pockets of magneto-sheath-like plasma in the mixing region. A more plausible interpretation is that the pockets represent detached regions of plasma, which have crossed the boundary, and that boundary crossings had taken place in both directions. Of course, this does not exclude the existence of a Kelvin Helmholz instability right at the boundary.

There is evidence for both open and closed filed lines in the LLBL (Scholer and Treumann, 1997) with a larger fraction of closed field lines during northward IMF conditions. Fujimoto *et al.* (1997, 1998) found that the mixing region plasma (cold-dense plasma) was accompanied by bi-directional flows of thermal electrons and proposed that the mixing region is on closed fieldlines while the sheath-like region is on open field-lines. Sauvaud *et al.* (1997), also found bi-directional electrons in a large part of the LLBL. Williams *et al.* (1985), during two northward IMF cases concluded that both the dawn and the dusk LLBL were completely on closed field lines. The open/closed problem has not yet been sufficiently investigated for this particular northward IMF event, but we can assume that the field-lines were certainly closed after 0300 UT and maybe also before that time.

The boundaries between the tailward drifting pockets of sheath-like plasma and the surrounding region of transverse-earthward drifting plasma are sites of strong shear. The magnetic field measurements show strong localised currents at these boundaries, as may be

expected. The strongest B-field variations in Fig. 13 are seen in the B_X component, in agreement with a mainly field-aligned current direction, that is a current direction essentially along the z axis. The B_Z signature in one of the events is bipolar, and such signatures are often interpreted as signs of plasmoids, but this identification would be premature at this stage.

The pockets of sheath-like plasma with their accompanying field-aligned currents appear to be related to the dispersion structures in the high altitude ionosphere. Woch and Lundin (1991) found the dispersion structures to be associated with localised field-aligned currents, and in the Interball-1 LLBL data the clearest field-aligned currents are the ones associated with the sheath-like plasma pockets. From the footpoint map in Fig. 12 it can be concluded that the clear dispersion structures are from a topological point of view more likely to map to the inner part of the LLBL than to the outer part. On the other hand, a source even further in is not likely either.

Woch and Lundin (1992a) computed a source distance for their dayside injection events of typically less than 10 R_E. Using the Tsyganenko 87 model they found that a majority of the events mapped to the magnetopause region at Z_{GSM} a few R_E away from the equator. For events before 7.5 MLT Z_{GSM} was typically 2–5 R_E. Our Interball-1 measurements were obtained at $Z_{GSM} \approx 4\,R_E$. Our calculated source distance was 15–20 R_E which falls somewhat short of the distance between Interball-2 and Interball-1, but the difference is not dramatic.

We would like to point out that there are at least two major problems with our suggested source region for which we so far have no answers. The first one is the spatial extent. We do not know the three-dimensional shapes of the pockets of sheath-like plasma. Are they elongated in their flow direction? This would lead to field-aligned current sheets elongated in this direction and would explain why most of the magnetic field variation is in the x-component. Do they map to ionospheric regions large enough for one dispersion structure? The second problem is temporal. How can these structures give a source which is switching on and off? These questions will be addressed in future studies.

Finally we would like to point out that PROMICS-3-Auroral has also measured dispersion structures above the evening side auroral oval. A spectacular case, with injection structures as far back as at 21 MLT, occurred on January 11, 1997 (Sandahl *et al.*, 1998).

4 Conclusions

In this study the PROMICS-3 hot plasma spectrometer on Interball-2 is described and two examples of initial results are presented.

The first example is an observation of upward flowing molecular ions above the nightside auroral oval at an unusually high energy, 600 eV. Upward flowing molecular ions have been detected by PROMICS-3-Auroral on a few occasions, both on the dayside and on the nightside, but such events are rare. The case presented occurred during an extended period of fairly high geomagnetic activity.

The second example is an event with nearly conjugate measurements by Interball-2 and Interball-1 of ion injection structures of magnetosheath origin above the morningside auroral oval and in the dawnside low-latitude boundary layer. This case occurred during quiet geomagnetic conditions when the IMF direction was weakly northward. At Interball-2 the injection structures were seen as dispersion events in the MLT range 0530–0830 at invariant latitudes 71–79°, the clearest dispersion structures appearing in the equatorward part of this range.

The LLBL was a mosaic of two different types of plasma, one sheath-like tailward streaming and one with a transverse-earthward flow direction. The sheath-like population dominated in the outer LLBL, but there were isolated pockets of the transverse-Earthward flowing population. In the inner LLBL this situation was reversed. The pockets of sheath-like plasma in the inner LLBL were associated with localised field-aligned currents, and we propose that there were associated with the dispersion structures in the ionosphere.

Acknowledgements. The major part of the hardware has been designed and built at the Swedish Institute of Space Physics in Kiruna. Much of the electronics has been built in Finland by the Finnish Meteorological Institute, Hollming OY, and VTT. PROMICS-3 is financed by grants from The Swedish National Space Board, The Royal Swedish Academy of Sciences, the Technology Development Center (in Finland) and the Academy of Finland. We would like to thank S. Romanov for kindly providing magnetic field data. The footpoint calculations used in Fig. 12 were carried out by V. Prokhorenko.

References

Budnick, E., A. Fedorov, and I. Sandahl, First results from mass-spectrometer PROMICS-3 in INTERBALL project (Auroral Probe), *Kosm. Issl.*, **36,** 73–85, 1998. English edition *Cosmic Res.*, 36, 68–80, 1998.

Carlson, C. W., and R. B. Torbert, Solar wind ion injections in the morning auroral oval, *J. Geophys. Res.*, **85,** 2903, 1980.

Craven, P. D., R. C. Olsen, C. R. Chappell, and L. Kakani, Observations of molecular ions in the Earth's magnetosphere, *J. Geophys. Res.*, **90,** 7599, 1985.

Förster, M., N. Jakowkski, A. Best, and J. Smilauer, Plasmaspheric response to the geomagnetic storm period March 20–23, 1990, observed by the ACTIVNY (MAGION-2) satellite, *Can. J. Phys.*, **70,** 569, 1992.

Fujimoto, M., T. Terasawa, and T. Mukai, The cold-dense plasma sheet: a geotail perspective, *Space Sci. Rev.*, **80,** 325, 1997.

Fujimoto, M., T. Mukai, H. Kawano, M. Nakamura, A. Nishida, Y. Saito, T. Yamamoto, and S. Kokobun, Structure of the low-latitude boundary layer: a case study with Geotail data. *J. Geophys. Res.*, **103,** 2297, 1998.

Galeev, A. A., Y. I. Galperin and L. M. Zelenyi, The INTERBALL project to study solar-terrestrial physics, in Interball mission and payload, CNES-IKI-RSA, p. 11, May 1995.

Hoffman, J. H., W. H. Dobson, C. R. Lippincott, and H. D. Hammack, Initial ion composition results from the Isis 2 satellite, *J. Geophys. Res.*, **79,** 4246, 1974.

Klecker, B., E. Möbius, D. Hovestadt, M. Scholer, G. Gloeckler, and F. M. Ipavich, Discovery of energetic molecular ions (NO^+ and

O_2^+) in the storm time ring current, *Geophys. Res. Lett.*, **13,** 632, 1986.

Mitchell, D. G., F. Kutchko, D. J. Williams, T. E. Eastman, L. A. Frank, and C. T. Russell, An extended study of the low-latitude boundary layer on the dawn and dusk flanks of the magnetosphere, *J. Geophys. Res.*, **92,** 7394, 1987.

Nemecek, Z., A. Fedorov, J. Safrankova, G. Zastenker, Structure of the low-latitude magnetopause: MAGION-4 observations, *Ann. Geophysicae*, **15,** 553, 1997.

Paschmann, G., B. U. Ö. Sonnerup, I. Papamastorakis, W. Baumjohann, N. Sckopke, and H. Lühr, The magnetopause and boundary layer for small magnetic shear: convection electric fields and reconnection, *Geophys. Res. Lett.*, **17,** 1829, 1990.

Sandahl, I., S. Barabash, E. M. Dubinin, H. Koskinen, R. Lundin, D. Obod, R. Pellinen, N. F. Pissarenko, T. Pulkkinen, B. Rautio, and A. V. Zakharov, The plasma composition spectrometer PROMICS-3 in the Interball project, in *Interball Mission and Payload*, CNES, IKI, RSA, p 178, May 1995.

Sandahl, I., S. Barabash, H. Borg, E. Y. Budnik, E. M. Dubinin, U. Eklund, H. Johansson, H. Koskinen, K. Lundin, R. Lundin, A. Moström, R. Pellinen, N. F. Pissarenko, T. Pulkkinen, P. Toivanen, and A. V. Zakharov, First results from the plasma composition spectrometer PROMICS-3 in the Interball project, *Ann. Geophysicae*, **15,** 542, 1997.

Sandahl, I., H. E. J. Koshinen, A. M. Mälkki, T. I. Pulkkinen, E. Y. Budnick, A. O. Fedorov, L. A. Frank, and J. B. Sigwarth, Dispersive magnetosheath-like ion injections in the evening sector on January 11, 1997, *Geophys. Res. Lett.*, **14,** 2569 1998.

Sauvaud, J-A., P. Koperski, T. Beutier, H. Barthe, C. Aoustin, J. J. Thocaven, J. Rouzaud, E. Penou, O. Vaisberg, N. Borodkova, The INTERBALL-Tail ELECTRON experiment: initial results on the low-latitude boundary layer of the dawn magnetosphere, *Ann. Geophysicae*, **15,** 587, 1997.

Savin, S. P., et al., Interball magnetotail boundary case studies, *Adv. Space Res.*, **20,** 999, 1997.

Scholer, M., and R. A. Treumann, The low-latitude boundary layer at the flanks of the magnetopause, *Space Sci. Rev.*, **80,** 341, 1997.

Sckopke, N., G. Paschmann, G. Haerendel, B. U. Ö. Sonnerup, S. J. Bame, T. G. Forbes, E. J. Hones, Jr., and C. T. Russell, Structure of the low-latitude boundary layer, *J. Geophys. Res.*, **86,** 2099, 1981.

Taylor, H. A., Jr., High latitude minor ion enhancements: a clue for studies of magnetosphere-atmosphere coupling, *J. Atmos. Terr. Phys.*, **36,** 1815, 1974.

Traver, D. P., D. G. Mitchell, D. J. Williams, L. A. Frank, and D. Y. Huang, Two encounters with the flank low-latitude boundary layer: Further evidence for closed field topology and investigation of the internal structure, *J. Geophys. Res.*, **96,** 21 025, 1991.

Williams, D. J., D. G. Mitchell, T. E. Eastman, and L. A. Frank, Energetic particle observations in the low-latitude boundary layer, *J. Geophys. Res.*, **90,** 5097, 1985.

Woch, J., and R. Lundin, Temporal magnetosheath plasma injections observed with Viking: a case study, *Ann. Geophysicae*, **9,** 133, 1991.

Woch, J., and R. Lundin, Signatures of transient boundary layer processes observed with Viking, *J. Geophys. Res.*, **97,** 1431, 1992.

Yau, A. W., B. A. Whalen, C. Goodenough, E. Sagawa, and T. Mukai, EXOS D (Akebono) observations of molecular NO^+ and N_2^+ upflowing ions in the high altitude auroral ionosphere, *J. Geophys. Res.*, **98,** 11 205, 1993.